# Front dynamics of a water surge at high Reynolds number: similarity solutions to the Saint-Venant equations

C. Ancey, S. Cochard, M. Rentschler, & S. Wiederseiner
*Ecole Polytechnique Fédérale de Lausanne, Ecublens, 1015 Lausanne, Switzerland*

In this paper, we seek similarity solutions to the shallow-water (Saint-Venant) equations for describing the motion of a gravity-driven surge supplied in fluid by a source placed at the inlet of a horizontal plane. Gratton and Vigo (1994) have shown that imposing certain conditions on the inflow rate makes it possible to find similarity solutions to the Saint-Venant equations when a Benjamin-like boundary condition is imposed at the froude (i.e., non-zero flow depth). When the flow depth is zero at the front, we show that the solution to the Saint-Venant equations is singular: its curve is the limiting curve of the regular solutions. We also show that the front takes the form of an acute wedge, with a straight free boundary, and is separated from the body by a bore. This singular behavior explains why current numerical models fail in computing the front position and velocity when no *ad hoc* downstream boundary conditions are supplemented.

## 1 INTRODUCTION

There is a growing number of models inspired from shallow-water (Saint-Venant) equations, which are used to describe time-dependent, free-surface flows involving fluids with various rheologies. Essentially, these models are based on a set of hyperbolic partial differential equations that are obtained by integrating the mass and momentum balance equations across the flow depth. Typical examples include density currents (Rottman and Simpson 1983), particle suspensions (Parker et al. 1986), viscoplastic fluids (Huang and Garcìa 1998), dry granular flows (Savage and Hutter 1989), saturated granular fluids (Iverson and Denlinger 2001), etc.

The models cited above have often been used to compute the collapse of a finite volume of fluid or the spread of a surge emanating from a source with a given inflow rate. The common characteristics of these flows is that they have a front exhibiting a significant curvature of the free surface. For an inertia-dominated regime, an *ad hoc* boundary condition must often be imposed at the front by constraining the value of the Froude number in order to take into account the resisting effect of the ambient fluid (Benjamin 1968). This is tantamount to considering the front as a discontinuity (bore) moving at a prescribed velocity. Using phase-plane formalism, Gratton and Vigo (1994) provided evidence that the front controls the dynamics of the body on some specific circumstances. A few analytical results have also been established without imposing this front condition: Ritter (1892) provided an analytical solution to the shallow-water equations for the dam-break problem. In that case, it was shown that the head was an elongating wave presenting an acute angle at the leading edge. Later, Dressler (1952) and Whitham (1954) demonstrated that hydraulic resistance modified the shape and velocity of the front. In addition to providing more rigorous proofs, Hogg and Pritchard (2004) found that taking shearing effects into account substantially alters the mathematical structure of the solution to the dam-break problem, especially in the tip region.

The objective of this paper is to find similarity solutions to the Saint-Venant equations in the context of rapidly varying surges emanating from a source and spreading along a horizontal plane. Similarity solutions were found in an earlier paper by Gratton and Vigo (1994), where these authors considered a Benjamin-like boundary condition at the front, i.e., the Froude number $Fr$ is constant and the flow depth is nonzero. Gratton and Vigo (1994) claimed that the solution associated with the boundary condition $h = 0$ is found by taking the limit $Fr \to \infty$. In this paper, we will show that the proper solution associated with a zero flow depth at the front is a singular curve, which structurally differs from the solutions related to a Benjamin-like boundary condition. Emphasis will be given to the topological structure of the equations in the tip re-

gion. It will be shown that the front dynamics is fully controlled by the critical points of the phase plane, implying that the shape and velocity of the tip region are imposed independently of the far-field conditions. We will show that the solutions found in this paper are in fairly good agreement with the analytical solutions to the Euler equations (Ancey et al. 2006).

## 2 GOVERNING EQUATIONS

### 2.1 *Flow-depth averaged equations*

We consider a shallow layer of fluid flowing over a rigid horizontal impermeable plane. The fluid is inviscid and incompressible; its density is denoted by $\rho$. The ratio $\epsilon = H_*/L_*$ between the typical vertical and horizontal lengthscales, $H_*$ and $L_*$ respectively, is assumed to be small. $U_* = O(\sqrt{gH_*})$ is the velocity scale.

Integrating the local Euler equations over the flow depth provides the shallow-water equations. Since they are classic, the details of their derivation are not reported here (Stoker 1957). The shallow-water equations take the generic dimensionless form

$$\frac{\partial h}{\partial t} + \frac{\partial h\bar{u}}{\partial x} = 0,$$

$$\frac{\partial h\bar{u}}{\partial t} + \frac{\partial h\overline{u^2}}{\partial x} + h\frac{\partial h}{\partial x} = 0,$$

where the bar refers to flow-depth averaged values. The dimensionless velocity, flow-depth, distance, and time were defined as $\bar{u} = \hat{u}/U_*$, $h = \hat{h}/H_*$, $x = \hat{x}/L_*$, and $t = \hat{t}U_*/L_*$, respectively, where the hat refers to dimensional variables. Introducing the Boussinesq coefficient $\gamma$ makes it possible to relate the mean square velocity to the square of the mean velocity: $\overline{u^2} = \gamma\bar{u}^2$. In so doing and assuming that $\gamma$ is known, we obtain a closed set of equations for $h$ and $\bar{u}$

$$\frac{\partial h}{\partial t} + \frac{\partial h\bar{u}}{\partial x} = 0, \tag{1}$$

$$\frac{\partial \bar{u}}{\partial t} + (2\gamma - 1)\bar{u}\frac{\partial \bar{u}}{\partial x} + \bar{u}^2\frac{\partial \gamma}{\partial x} = -\frac{\partial h}{\partial x}\left(1 + \frac{\bar{u}^2}{h}(\gamma - 1)\right). \tag{2}$$

When $\gamma$ is set equal to unity in the momentum balance equation (2), we retrieve the usual form of the shallow-water equations (Stoker 1957). When $\gamma$ is constant and in excess of unity, the conservation form of Eqs. (1–2) is identical to the equations used by Hogg and Pritchard (2004) to analyse the effect of shear on front structure. In that case, the structure of the governing equations is slightly altered: the convective acceleration term is weighted by the shape factor $2\gamma - 1$, while a Chézy-like term affects the pressure gradient. These modifications are minor and do not disturb the hyperbolic nature of the equations; they may, however, have significant impact on some occasions, e.g. when computing the nose features in the dam-break problem (Hogg and Pritchard 2004). A pervasive assumption is to ascribe the Boussinesq coefficient to unity by advocating that in the high Reynolds number limit, the velocity profile is blunt, which implies that $\gamma$ must not differ significantly from unity.

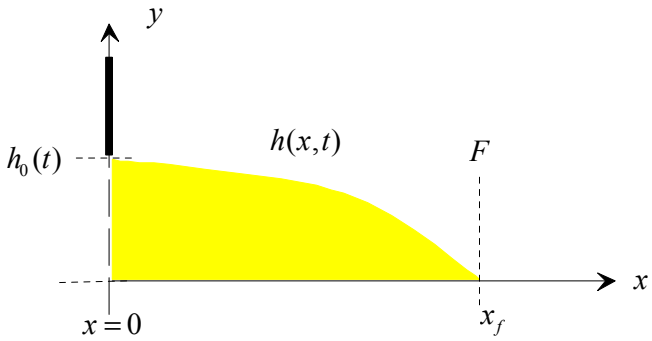


Figure 1. The configuration of the flow.

### 2.2 *Flow geometry and boundary conditions*

A two-dimensional flow regime is assumed, namely any cross-stream variation is neglected. The depth of the layer is given by $h(x, t)$ (see Figure 1). The flow is generated by a source of fluid: at $t = 0$, the sluice gate at the inlet is raised with a given aperture rate $h_0(t)$. Ahead of the front, there is a dry bed.

At the source $x = 0$, the boundary condition is given by the relation

$$\mathcal{V} = \int_0^{x_f} h(x, t)dx = At^n, \tag{3}$$

with $n$ a prescribed coefficient; in the forthcoming numerical applications, we will take $n = 5/2$. The boundary condition (3) is equivalent to imposing the flow rate at the inlet: $\bar{u}h = nAt^{n-1}$. To get rid of the initial-value problem, we furthermore assume that the Froude number at the source is imposed: $Fr_0 = \bar{u}/\sqrt{h} = 2a/3$, where $a$ is a constant. The flow depth varies with time: $h = h_0(t) = at^m/d$, where $m = \frac{2}{3}(n - 1)$ ($m = 1$ in the numerical applications here, since $n = 5/2$). Note that $d$ and $a$ are linked: they both related through the relation $A = \frac{2}{3n}a^{5/2}d^{-3/2}$ (this relation is found by integrating the solution to find the volume).

The other boundary conditions is prescribed at the front. The front position $x_f$ is the point where the flow depth drops to zero: $h(x_f) = 0$; moreover, the front velocity is $\bar{u}(x_f) = \dot{x}_f$.

### 2.3 *Jump conditions*

The solutions to the system (1–2) may admit discontinuities (shock or hydraulic jump in the hydraulic

literature). The flows either side of these are connected by jump conditions which express conservation of mass and momentum across the moving discontinuity. Denoting the shock speed by $\sigma$, these jump conditions associated with conservative form of Eqs. (1–2) are given by (Whitham 1974)

$$[\![h\bar{u}]\!] = \sigma[\![h]\!], \tag{4}$$

$$[\![\gamma h\bar{u}^2 + h^2/2]\!] = \sigma[\![h\bar{u}]\!], \tag{5}$$

where the $[\![\cdot]\!]$ denotes the difference upstream and downstream of the shock.

## 3 PHASE-PLANE FORMALISM

In order to solve the similarity problem, we will use the 'phase-plane' (or portrait) formalism as earlier authors did for the same kind of problem (Grundy and Rottman 1986; Gratton 1991; Gratton and Vigo 1994). The types and characteristics of the similarity solutions are described in details by Gratton and Vigo in (Gratton and Vigo 1994) when the downstream boundary condition is of the Benjamin type, i.e., at the front, the Froude number is constant and the flow depth is nonzero. Gratton and Vigo claimed that the boundary condition $h(x_f) = 0$ is obtained asymptotically by making the Froude number tend to infinity (Gratton and Vigo 1994), but we will show that in the particular case investigated here, their construction is not possible. Except for this point, the formalism is identical to that used in (Gratton and Vigo 1994) and we will not replicate their results. This notably implies that we will focus on a single particular case $n = 5/2$ in our applications for clarity (the other cases being similar).

Gratton and Vigo (1994) have shown that the governing equations (1–2) admit similarity solutions for a range of conditions at the source $0 \leq n < 4$. This condition on $n$ is needed for the shallowness assumption to be consistent. Following Grundy and Rottman (1986) and Gratton and Vigo (1994), we pose

$$u = \delta\xi t^{\delta-1} V(\xi),$$
$$h = \delta^2\xi^2 t^{2(\delta-1)} Z(\xi),$$
$$\xi = \frac{x}{t^\delta},$$

with $\delta$ to be determined from the initial conditions (3). The boundary conditions impose

$$Z(\xi_f) = 0 \text{ and } V(\xi_f) = 1, \tag{6}$$

where $\xi_f$ denotes the front position. At the source, we have the asymptotic behaviour

$$Z \propto \frac{a}{d}\frac{1}{\delta^2\xi^2} \text{ and } V \propto \frac{2}{3}\frac{a^{3/2}}{\sqrt{d}}\frac{1}{\delta\xi} \text{ when } \xi \to 0. \tag{7}$$

Since the solution may admit discontinuities, we supplement the following condition derived from Equation (3), which ensures that the mass balance is not violated

$$\int_0^{\xi_P} \xi^2 Z(\xi) d\xi = \delta^{-2}\mathcal{V}, \tag{8}$$

with $\mathcal{V}$ the total volume and $\xi_P$ the front abscissa. When there is not discontinuity, this equation is redundant with Equation (7).

## 4 SIMILARITY SOLUTIONS

We shall see that $\xi$ is an autonomous variable in the governing equations for $Z$ and $V$, which means that we can get rid of $\xi$ and directly seek a relation between $Z$ and $V$ by solving a first-order ordinary differential equation in the form

$$\frac{dZ}{dV} = \frac{F(V, Z)}{G(V, Z)}. \tag{9}$$

The behaviour of the solutions to this equation can be qualitatively outlined by working in the $V - Z$ plane and discussing the various possibilities of finding an 'integral' curve passing through a given region.

### 4.1 *Matrix representation and critical curves*

Substituting the similarity forms into the governing equations (1–2), we obtain two ordinary first-order differential equations for $Z$ and $V$ that can be cast in a matrix form

$$\mathbf{M}(V, Z)\frac{d\mathbf{w}}{d\xi} = \frac{Z}{\delta\xi}\mathbf{S}(V, Z), \tag{10}$$

with $\mathbf{w} = [Z, V]^{\mathrm{T}}$,

$$\mathbf{M} = \begin{bmatrix} V - 1 & Z \\ (\gamma - 1)V^2 + Z & Z(V(2\gamma - 1) - 1) \end{bmatrix}, \text{ and}$$

$$\mathbf{S} = \begin{bmatrix} 3V\delta - 2 \\ 2\delta Z + V(V(4\gamma - 3)\delta - 1) \end{bmatrix}.$$

The determinant of the matrix $\mathbf{M}$ is

$$\det\mathbf{M} = \delta Z\left(Z - I(V)\right),$$

with $I(V) = 1 + (V - 2)V\gamma$. Along the $V$-axis ($Z = 0$) and the curve $C_I$ of equation $Z = I(V)$, the solutions $V(\xi)$ and $Z(\xi)$ to Equations (10) are not properly defined because $\det\mathbf{M} = 0$: these functions are multivalued except when the crossing occurs close to a critical point. A multivalued behaviour is not physically admissible and this issue is fixed by constructing discontinuous solutions (see Section 5).

When $\det\mathbf{M}$ is nonzero, the system of equations (10) can be inverted to provide

$$\xi\frac{dZ(\xi)}{d\xi} = \frac{F(V, Z)}{\delta\left(Z - I(V)\right)}, \tag{11}$$

$$\xi \frac{dV(\xi)}{d\xi} = \frac{G(V,Z)}{\delta\,(Z - I(V))}. \qquad (12)$$

Instead of solving this system of differential equations, we form the ratio of the two equations to arrive at a single ordinary differential equation (9) for $Z'(V)$.

When $\det \mathbf{M}$ is zero, the system may have solutions if the determinant of the cofactor matrix

$$\mathbf{N} = \begin{bmatrix} V-1 & 3V\delta - 2 \\ (\gamma-1)V^2 + Z & 2\delta Z + V(V(4\gamma-3)\delta - 1) \end{bmatrix},$$

is also zero. In the space ($V$, $Z$), the locus of the points for which $\det \mathbf{N} = 0$ is a continuous curve $C_J$ of the equation

$$Z = J(V) = \frac{V\,(\gamma\delta V^2 + (-4\delta\gamma + 2\gamma + 3\delta - 3)V + 1)}{(V+2)\delta - 2}.$$

Note that $G(V, Z) = Z - J(V)$, which means that $C_J$ is also the locus of points where the integral curves, solutions to Equation (9) have vertical tangents. Except for the case $\gamma = 1$ and $n = 1$ ($\delta = 1$), the curves $C_I$ and $C_J$ do not coincide, but intersect at two points: $A_\gamma$ with coordinates $(2/(4\gamma-3), (9-8\gamma)/(4\gamma-3)^2)$ and $P_*$ with coordinates $(1, 1-\gamma)$. $P_*$ lies inside the first quadrant only when $\gamma \leq 1$. These points play an important role since their existence means that there may be continuous solutions with discontinuous gradients at points A and $P_*$. They will be useful thereafter in constructing the solutions (see Section 5). When $\gamma = 1$ and $n = 1$ corresponding to the dam break problem (Whitham 1974), the curves $C_I$ and $C_J$ coincide, which implies that a piece of this curve is a part of the solution sought.

### 4.2 *Critical points*

In addition to the curves $C_I$ and $C_J$, there is another specific curve that plays a role in the phase portrait: the curve $C_F$ is the curve along which $F$ vanishes, i.e. at which the integral path has a horizontal tangent; its equation is given by

$$H = \frac{2 + U\,(3 - 3\,\delta + 2\,\gamma\,(-2 + U\,\delta))}{2\delta}.$$

There are three critical points resulting from the crossing of the specific curves $C_F$ and $C_J$. The first one is the origin point O, which is a node. Point $A_\gamma$ is also a singularity (node). The third one is referred to as point $B_\gamma$ and has coordinates $(2/(3\delta), (9-8\gamma)/(9\delta^2))$; it is a saddle.

Figure 2 shows a few trajectories, the specific curves ($C_I$, $C_J$, and $C_F$), the critical points (O, $A_\gamma$, $B_\gamma$), the intersection point $P_*$ between $C_I$ (solid line) and $C_J$ (dashed line), and the front $P$. Note that at point $A_\gamma$, the three curves $C_I$, $C_J$, and $C_F$ meet, which implies significant behaviour changes close to point $A_\gamma$. A few trajectories (thin curves with arrows) representing solutions to Equation (9) are also reported and illustrate the behaviour of the solutions close to the critical points; not all the paths are physically meaningful since some cross the critical curve $C_I$ (solid line).

## 5 FLOW DISCONTINUITIES

### 5.1 *Rankine-Hugoniot condition*

The crossing of the critical curve $C_I$ at a regular point of intersection is not possible, but is possible at a critical point ($A_\gamma$ here). When the crossing is not permitted, we consider that a shock occurs, which is ruled by the jump conditions (4–5). If we know the flow variables $Z_1$ and $V_1$ upstream (respectively, downstream) of the shock, we can solve the shock equations (4–5) to determine the shock velocity $\sigma$ and a curve referred to as the 'shock curve' $V_2(Z_2|Z_1, V_1)$, which is the locus of all the points satisfying the jump conditions (4–5). Solving this system of equations, we derive the shock velocity and the variation in upstream velocity $V_2$ with upstream flow depth $Z_2$

$$\sigma = \frac{\gamma}{\chi} V_1 \pm \frac{1}{\chi}\sqrt{\frac{1}{2}\left(\chi(Z_1+Z_2) + 2(\gamma-1)V_1^2\right)\frac{Z_2}{Z_1}}, \qquad (13)$$

$$V_2(Z_2|Z_1, V_1) = \frac{V_1}{\chi} \pm \qquad (14)$$

$$\frac{(Z_2 - Z_1)}{\chi}\sqrt{\frac{1}{2}\frac{\chi(Z_1+Z_2) + 2(\gamma-1)V_1^2}{Z_1 Z_2}},$$

with $\chi = \gamma + (1-\gamma)\frac{Z_2}{Z_1}$. Since there is a quadratic dependence on velocity in Eqs. (4–5), we actually find two shock curves, but a single one is physically admissible by requiring that energy dissipation through the shock be positive. This shock curve is then used to pass from one trajectory to another one that satisfies the boundary conditions downstream (respectively, upstream). The problem boils down to finding the point ($V_1$, $Z_1$) at which the shock occurs. To that end, we use a trial and error procedure: first we select a point ($V_1$, $Z_1$) on the integral path emanating from the source S, then we plot the shock curve $V_2(Z_2|Z_1, V_1)$, and finally we find the intersection point between the shock curve and the other integral path coming from the front point P. The procedure is iterated until the fluid volume found by numerical integration is consistent by the inflow rate imposed at the plane entrance Equation (8).

### 5.2 *Weak discontinuities*

It is worth recalling that a particular case of discontinuity includes the functions that are continuous, but

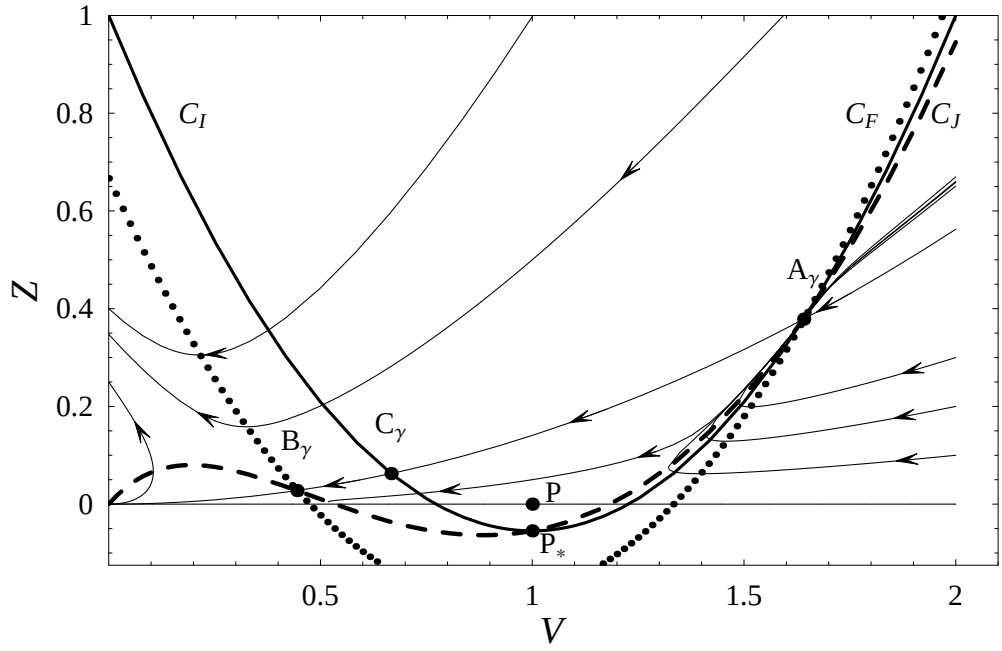


Figure 2. Specific curves $C_I$ (solid line), $C_J$ (dashed line), $C_F$ (dotted line). The thin curves with arrows represent a few trajectories computed numerically. The critical points O, $A_\gamma$ , $B_\gamma$, and $C_\gamma$ are plotted together with the front (point P). Computations made for $a = 4$, $d = 1$, and $\gamma = 1.05$.

whose derivative is not continuous at isolated points. This case is encountered when the curves $C_I$ and $C_J$ coincide (i.e. for $\gamma = 1$ and $n = 1$): when an integral curve crosses the critical curve, we have both $\det \mathbf{M} = 0$ and $\det \mathbf{N} = 0$, which implies that at this point, we can pass from one trajectory to another one and since $\det \mathbf{N} = 0$, the new trajectory is a piece of $C_I$ (Gratton and Vigo 1994).

## 6 SIMILARITY SOLUTIONS FOR $\gamma > 1$

We first consider the case where the Boussinesq coefficient is prescribed in advance. We are interested in determining the solutions to Equation (9) evolving in the first quadrant ($V \geq 0$, $Z \geq 0$) and related to $\gamma > 1$ and boundary conditions (6–8).

To simplify presentation, computation and numerical applications were made by taking $n = 5/2$ and $\delta = 3/2$.

### 6.1 *Special solution*

Note that there is a special analytical solution

$$Z = \frac{1}{4}(9 - 8\gamma)V^2, \tag{15}$$

which is the solution to Equation (9). This curve is a parabola that we call $\mathcal{P}$; the boundary condition (7) implies that the source point S lies at infinity on $\mathcal{P}$. No computation at this stage is needed since the corresponding integral path coincides with the special curve $\mathcal{P}$. As shown in Figure 2, $\mathcal{P}$ crosses the critical curves $C_I$ and the specific curve $C_J$ at point $A_\gamma$. Since this point is singular, the crossing is not associated with a hydraulic jump. A bit farther, the parabola once again crosses the curve $C_I$ at point $C_\gamma$ with coordinates $(2/3, 1 - 9\gamma/8)$, which is a regular point, implying that the solution should become discontinuous in the neighbourhood of $C_\gamma$. The parabola $\mathcal{P}$ does not pass through point P. Since the integral curve crosses the critical curve $C_I$, discontinuous solutions can be constructed. We then have two possibilities to envisage.

### 6.2 *Trajectories in the front neighborhood*

The first possibility occurs that, when reaching point $A_\gamma$ (for which $\det \mathbf{M} = \det \mathbf{N} = 0$), the integral curves take another path to reach point P. Since $A_\gamma$ is also a node, all the curves (except for the singular curves) are tangent to a limiting curve $C_A$, whose equation is given in terms of a Taylor expansion

$$Z = \frac{9 - 8\gamma}{(4\gamma - 3)^2} + \tag{16}$$

$$\left(V - \frac{2}{4\gamma - 3}\right) \frac{-16\gamma^2 - 4\delta\gamma + 24\gamma + 9\delta - 9}{2(4\gamma - 3)(4\delta\gamma - 4\gamma - 2\delta + 3)} +$$

$$+ O(V^2).$$

This equation is obtained by applying L'Hôpital's rule to Equation (9). Note that in numerical applications, we used a power series expansion to order $O(V^6)$ that ensures accuracy to within $10^{-4}$ in the numerical solution. Except when $\gamma = 1$, this limiting curve does not

pass through P. A graphical representation of $C_A$ is given in Figure 3 (dotted line). Since P is a regular point, a single integral curve passes through it: it is the trivial solution $Z = 0$ (the $V$-axis). The situation is sketched on Figure 3(a): no integral curve except for the trivial solution $Z = 0$ passes through point P representing the front. We conclude that there is no way of joining $A_\gamma$ and P when $\gamma \neq 1$ by following pieces of integral curves representing regular solutions to Equation (9).

The second possibility occurs when the parabola meets the critical curve $C_I$ at $A_\gamma$ or $C_\gamma$, which would make it possible to use the hydraulic jump conditions (13–14) to find another admissible integral curve. This is not possible because a hydraulic jump cannot form between a dry bed and the current, as mentioned above in solving the Euler equations. Indeed, using the shock conditions (13–14) to relate P to the integral path coming from S leads to constructing a nonphysical solution since the energy balance equation is violated. Point P can in no way can be located on a shock curve.

### 6.3 *Construction of the solution within the tip region*

None of these possibilities being effective, we must find another way of constructing the solution. A reasonable assumption is to consider that in the vicinity of the front, the Boussinesq coefficient drops to unity, which ensures that we can find a non-trivial integral path passing through P: the limiting curve $C_A$, as shown in Figure 3(b) is the only one passing through P except for the trivial solution. We construct the solution as follows. At point $A_\gamma$, the flow undergoes a shock: in the phase plane, this implies that there must be a shock curve mapping point $A_\gamma$ onto another point of the limiting curve $C_A$ that we refer to as point A'. This situation is depicted in Figure 3(b) and Figure 4(a). On Figure 4(a), we have plotted the two shock curves (long-dashed curve) emanating from $A_\gamma$ using Eqs. (13–14) together with points $A_\gamma$ and A'; the only physically admissible shock curve is that corresponding to a flow depth increase and a velocity decrease to ensure energy dissipation. Between A' and P, the integral path follows the limiting curve $C_A$. We can now compute the solution.

Since the integral path S$\rightarrow A_\gamma$ is given by Equation (15), we can analytically compute $V(\xi)$ by integrating Equation (12); we obtain: $\ln \xi^2 = \ln(9V - 4) - 3 \ln V + e$, where $e$ is a constant of integration. Taking into account the asymptotic behaviour when $\xi \rightarrow 0$ given by Equation (7), we deduce

$$\xi_A = \frac{\sqrt{2a^6 - 9a^4 + 27}}{2a^{3/2}\sqrt{3d\delta}}.$$

The path A'$\rightarrow$ P must be integrated numerically. For instance, for $a = 4$, we find $\xi_A = 1.850$ using the relation just above, $\xi_P - \xi'_A = 1.284$, which leads to $\xi_P = 3.133$. The fluid volume $\mathcal{V}$ is found by numerical

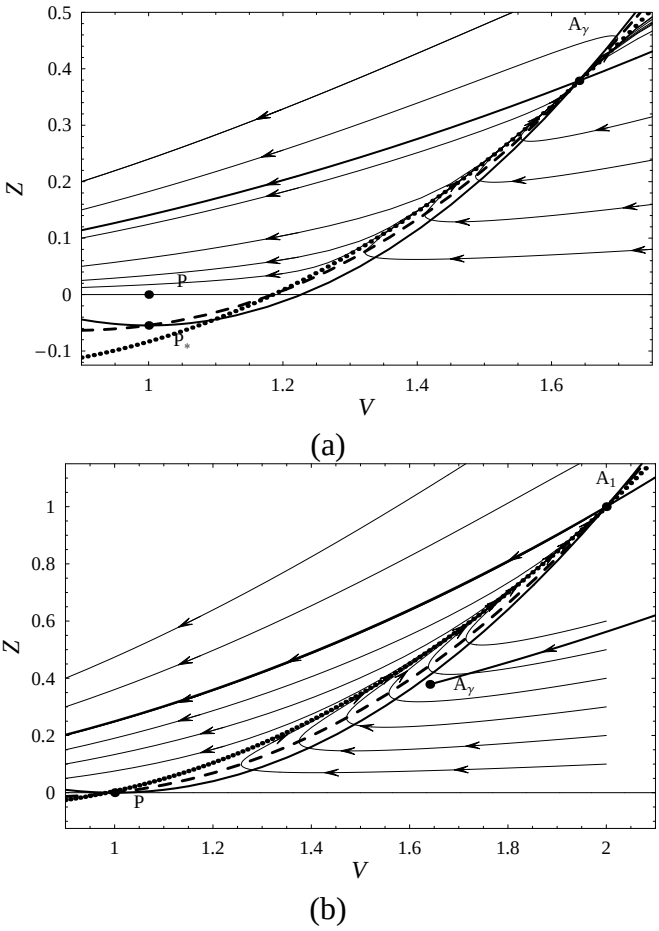


Figure 3. Specific curves $C_I$ (solid line), $C_J$ (dashed line) together with $C_A$ (dotted line). (a) Computations made for $a = 4$, $d = 1$, and $\gamma = 1.05$. (b) Computations made for $\gamma = 1$. The thin curves with arrows represent a few trajectories computed numerically; the arrows indicate increasing $\xi$. The critical point $A_\gamma$ (respectively $A_1$ in subplot b) is plotted together with the front P. The parabola $\mathcal{P}$ is a special trajectory and is plotted in bold; in subplot b, we have also superimposed the parabola $\mathcal{P}$ computed with $\gamma = 1.05$ and ending at $A_\gamma$.

integration of $\int_0^{x_p} h(x)dx$ and we find $\mathcal{V} = 8.516t^{5/2}$, which is very close to the exact variation imposed by Equation (8), i.e. $\mathcal{V} = 8.533t^{5/2}$ (relative error of $-0.2\%$). Better agreement can be obtained by considering that the critical transition occurs just upstream of point $A_\gamma$; e.g. for $a = 4$, the numerical computation (not reported here) showed that the transition occurs at $\xi_A = 1.738$ instead of $\xi_A = 1.850$.

## 7 SIMILARITY SOLUTION FOR $\gamma = 1$

We are now interested in determining the solution to Equation (9) in the usual case for the Saint-Venant equations, where the Boussinesq coefficient is set equal to unity. The resulting integral path in the phase plane continues to evolve in the first quadrant ($V \geq 0$, $Z \geq 0$) and must satisfy the boundary conditions (6–8). We still take $n = 5/2$ for the computations.

The general numerical solution of the problem represented by Equation (9) and boundary conditions (6–8) involves computing the solution from the source $S$ to the front $P$. Given the asymptotic behaviour exhibited by Equation (7), the source is located at infinity on a parabola of equation $Z = (V/\mathcal{F}_0)^2$, where $\mathcal{F}_0 = \frac{2}{3}a$ denotes the Froude number at the inlet. For numerical purposes, we need to give finite values $(V_0, Z_0)$ to the coordinates of the source point S in the phase plane. Taking large values for the initial value $V_0$ and posing $Z_0 = (V_0/\mathcal{F}_0)^2$ allows us to reasonably approximate the behaviour close to the source; typically taking $V_0 = 10^4$ is sufficient to obtain solutions accurate to within $10^{-4}$ close to the inlet. Equation (9) is solved numerically by moving from the source $S_0$ to the front P. The goal is to find an integral curve reaching point P.

As previously, there is no integral path relating the source point S and the front point P. Moreover, we suspect the occurrence of a jump. Indeed, the topological structure of the phase plane is a bit different compared to the case $\gamma > 1$, since the integral path does not pass through the critical point $A_1$ in the supercritical region and thus crosses the critical curve $C_I$ at a regular point that we refer to as R.

To construct the solution with a discontinuity, we have used the trial and error procedure, as specified in Section 5. As earlier, we note that the only trajectory coming from P is the limiting curve $C_A$. We then assume that a piece of the path P→$A_1$ on this curve is a part of the solution sought; the other part of the solution is a piece of the integral path S→R. On this latter curve, we guess the position of the point marking the discontinuous transition towards the path P→$A_1$; we refer to this point as point E. At regular point E, there is a jump. As a typical example, we have plotted the shock curves (long-dashed line) on Figure 5(a); a single curve crosses the limiting curve emanating from P and we refer to this intersection point as E'.

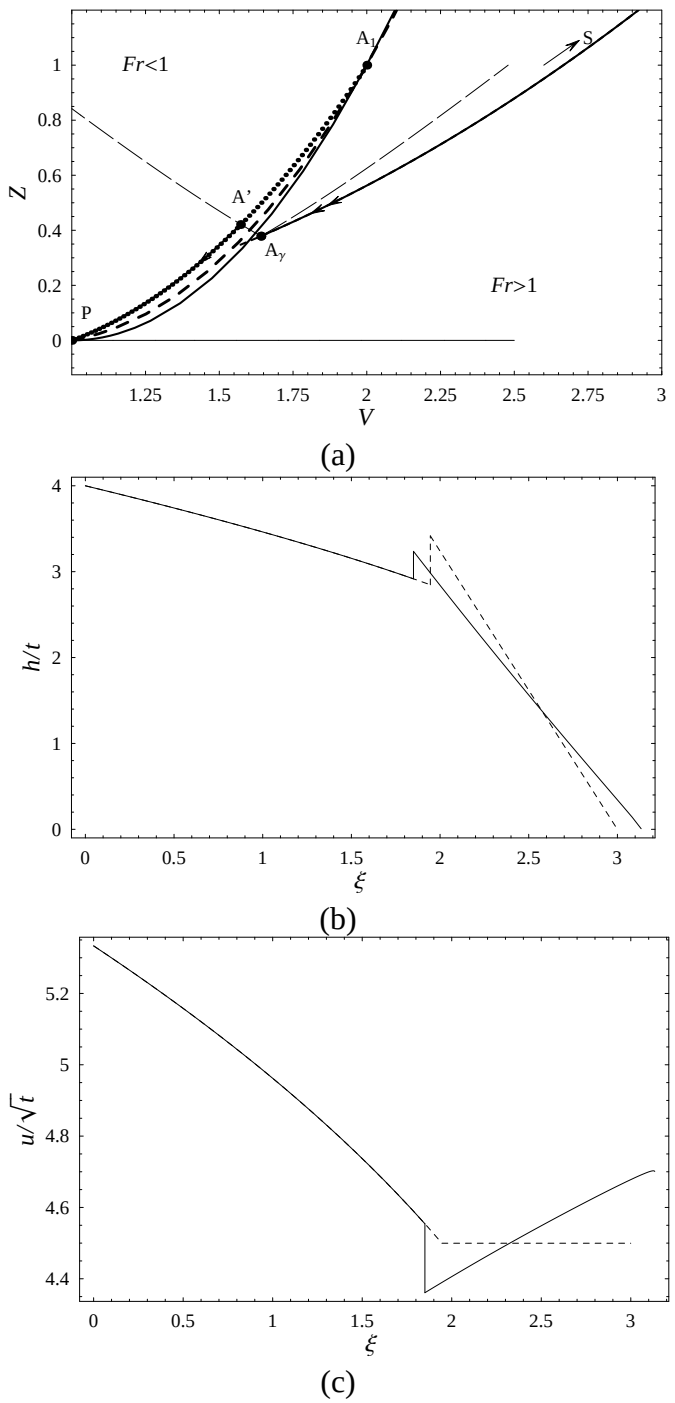


Figure 4. (a) Phase plane in the vicinity of $A_\gamma$: the specific curves $C_I$ (solid line), $C_J$ (dashed line), $\mathcal{P}$ (dotted line) are reported. The critical point $A_\gamma$ is plotted together with the front P. The long dashed lines represent the shock curves emanating from point $A_\gamma$. (b) Flow-depth variation with $\xi$: the solution to the Saint-Venant equations (solid line) is compared with the solution to Euler equations (dashed line). (c) Velocity variation with $\xi$. All the computations made for $a = 4$, $d = 1$, and $\gamma = 1.05$.

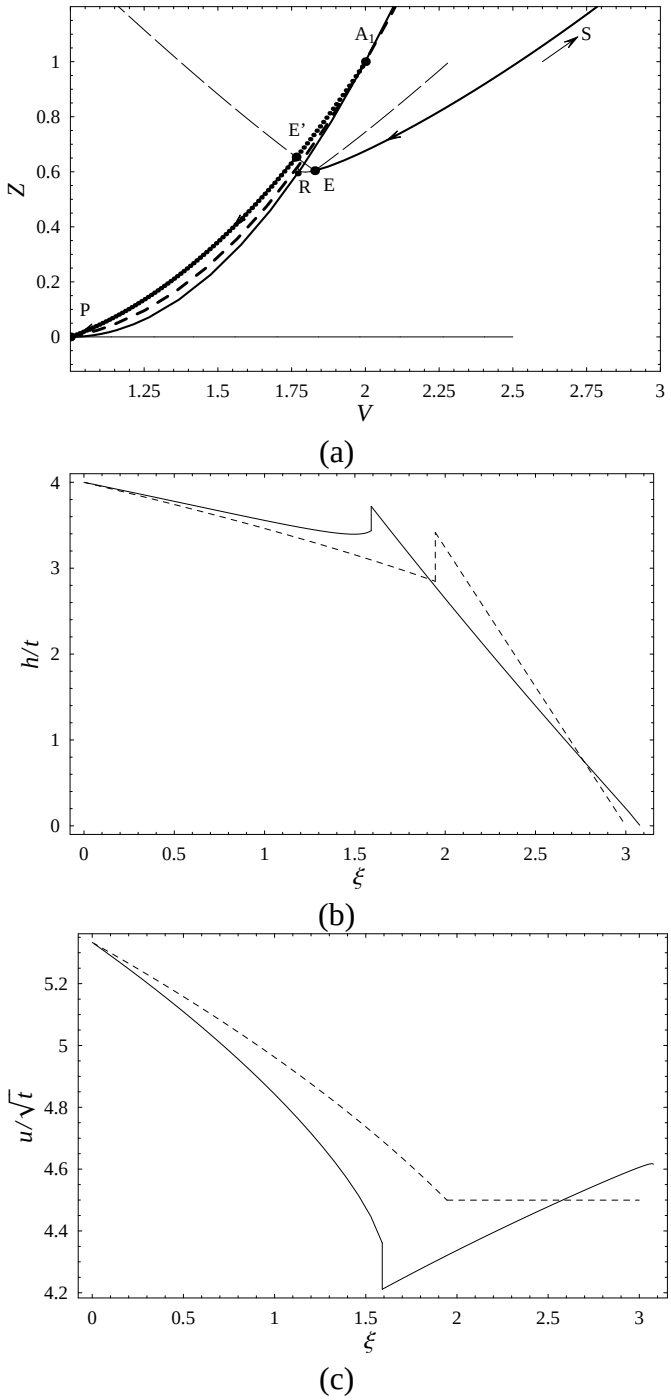


Figure 5. (a) phase plane in the vicinity of $A_1$ and construction of the transition point E and its conjugate E'. Same caption as in Figure 4(a). (b) Flow-depth variation with $\xi$: the solution to the Saint-Venant equations (solid line) is compared with the solution to Euler equations (dashed line). (c) Velocity variation with $\xi$. All the computations made for $a = 4$, $d = 1$, and $\gamma = 1$.

The path EE' represents the jump experienced by the surge; the path PE' is the integral path representing the head while the path ES is the integral curve representing the body. Equations (12) and (9) have been numerically integrated to produce $Z(\xi)$ and $H(\xi)$. For instance, for $a = 4$ and $d = 1$, we found: $\xi_P = 3.077$, $\xi_E = 1.590$ versus $\xi_a = 2.999$ and $\xi_b = 1.945$ for the reference solution given in Paper I, $\xi_P = 3.133$ and $\xi_A = 1.850$ for the Saint-Venant solution related to $\gamma > 1$. The fluid volume $\mathcal{V}$ is found by numerical integration of $\int_0^{x_p} h(x)dx$, and we find $\mathcal{V} = 8.533t^{5/2}$, which perfectly matches the fluid volume imposed by Equation (3). It is also worth noting that the solution thus built is sensitive to the numerical estimation of the transition point E: changing the position of the endpoint E by a few percent along the curve SR leads to altering the fluid volume, which shows that there is only one solution for a given set of boundary conditions, at least locally. Similarly to the case $\gamma > 1$, we applied the same shock conditions as used by (Gratton and Vigo 1994) instead of the Rankine-Hugoniot relations (13–14) and again we obtained a solution that differed slightly from the solution given here: indeed, we found $\xi_P = 3.072$, $\xi_A = 1.593$, and $\mathcal{V} = 8.512t^{5/2}$ (i.e. relative deviation of $-0.3\%$ with the input volume).

On Figure 5(b–c), we have reported the flow-depth and velocity variations with the similarity variable $\xi$ (solid lines). We have also reported the reference solution (dashed lines) found in another paper (Ancey et al. 2006). Note the significant difference in the position of the transition point between the solutions, whereas the front position is properly evaluated to within 5%. In contrast, the departure from the theoretical curve remains moderate since the relative deviation doe not exceed 10% for the velocity and the flow depth.

## 8 DISCUSSION

A striking feature of our results is that the head of the surge is wedge-shaped with an acute angle. This wedge structure has been observed in experimental realizations of gravity currents in tanks. Different examples drawn from various flow conditions in the laboratory and in nature clearly demonstrate the existence of wedge-like fronts contrasting with the Benjamin assumption. For instance, in the experiments conducted by Simpson (1972) [see also (Simpson 1987)], the development of the flow patterns were made visible by using a blend of dense fluid and fine aluminium particles: a stretching vortex occupying the tip region was clearly observed at the leading edge and produced an intense roll-up of fine aluminium particles, which makes it possible to visualize the streamlines and the two vortices; in the upper part of the head, a counter-clockwise rotating vortex occurred.

This flow pattern is very close to the one exhibited by the Saint-Venant equations.

In most gravity-current models, the details of the front shape and structure are omitted and the front is replaced by something close to a hydraulic jump and ruled by a Benjamin-like relation according to which the Froude number at the front is a function of the relative submersion of the current and the density ratio between the current and the surrounding fluid. This boundary condition produces currents with a very narrow vertical front, which may appear unrealistic in some circumstances. This is the case of currents with an increasing flow rate, as studied here, where it has been shown that the head occupies one third of the total current length and adopts a wedge shape. The actual shape of the front has drawn little attention so far. In his seminal paper, Benjamin (1968) supplemented the earlier heuristical analysis of von Kármán, demonstrating that a steady front makes an angle of $\pi/3$ with respect to the horizontal: Benjamin provided an approximate analytical solution describing the shape for the lock-exchange problem when the flow depth is half the total depth and again found that the front angle was $\pi/3$. Recently, McElwaine (2005) has extended Benjamin's results by considering steady finite-volume currents down a steep slope, which experience resistance from the surrounding fluid. He also found that the front makes an angle $\pi/3$ with the bottom line. Our result contrasts with the earlier findings: the front angle is not constant, but varies with time. Therefore, there appear to be significant changes in dynamics in the front angle between steady and time-dependent flow conditions. This observation may have a potential impact since until now, most models have used a constant-Froude-number boundary condition even though the flow is not steady.

When compared to analytical solutions to the Euler equations (Ancey et al. 2006), the Saint-Venant equations successfully capture the shape and the dimensions of the front when the Boussinesq coefficient $\gamma$ is known in advance. In the converse case, when $\gamma$ is set equal to unity, the front shape is properly predicted, but its dimensions are slightly overestimated. This clearly shows that minute changes in the value of $\gamma$ markedly affect the solution to the Saint-Venant equations, as shown earlier by (Hogg and Pritchard 2004) in the case of a surge induced by a dam break. Surprisingly, whatever the value of $\gamma$, the front position is properly evaluated to within $4\%$. On the whole, despite the potential pitfalls of the problem investigated (strong time dependence, non-hydrostatic pressure, rapid regime transition), we can consider that the Saint-Venant equations provide very satisfactory results, even in the usual case where the Boussinesq coefficient is set equal to unity, since the relative deviation with the solution to the Euler equation usually does not exceed 10%.

## 9 CONCLUSION

The goal of this paper was to find similarity solutions to the Saint-Venant (shallow-water) equations when the boundary conditions at the front impose a zero flow-depth. The solutions to the Saint-Venant equations were constructed by making use of the phase-plane formalism and seeking similarity forms in a way similar to earlier investigations (Gratton and Vigo 1994).

When the Boussinesq coefficient was in excess of unity, it was not possible to find a physically admissible solution close to the front without providing further information. This conclusion is akin to the observation made by Hogg and Pritchard (2004) in their investigation of drag influence on head shape for the dam-break problem. Instead of using a Benjamin-like condition at the front (imposing a nonzero flow depth), we assumed that the flow-depth averaged velocity was uniform, which implied that the Boussinesq coefficient dropped to unity.

A very important point that did not seem to be noted in the previous investigation was that the only way to construct the solution close to the front was to determine a special curve, referred to as $C_A$ in the phase-plane analysis. Indeed, in the phase plane $V - Z$ (e.g. see Figure 2), the integral path representing the solution must pass through certain points; the front was represented by point P and laid in the neighborhood of a critical point called A, which was a node: all the curves in a given region around A were attracted by A and pass through it tangent to an asymptotic curve $C_A$. None of these integral paths passed through A, but the limiting curve $C_A$ did. This curve represented an *exceptional* and local solution to the Saint-Venant equations.

It is worth noticing that this topological structure of the similarity solutions in the front vicinity entails that a specific numerical method must be used to compute accurate solutions to Saint-Venant equations close to the front and explains why the current numerical methods fail to predict the behavior close to the front.

## Références


Ancey, C., S. Cochard, S. Wiederseiner, and M. Rentschler (2006). Similarity solutions for a gravity current in the high Reynolds-number Limit. (1) Euler equations. *Phys. Rev. E*, submitted.

Benjamin, T. (1968). Gravity currents and related phenomena. *J. Fluid Mech. 31*, 209–248.

Dressler, L. (1952). Hydraulic resistance effect upon the dam-break functions. *J. Res. Natl Bur. Stand. 49*(3), 217–225.

Gratton, J. (1991). Similarity and self similarity in fluid dynamics. *Fund. Cosmic Phys. 15*, 1–106.

Gratton, J. and C. Vigo (1994). Self-similar gravity currents with variable inflow revisited: plane currents.

*J. Fluid Mech. 258*, 77–104.

Grundy, R. and J. Rottman (1986). Self-similar solutions of the shallow-water equations representing gravity currents with variable inflow. *J. Fluid Mech. 169*, 337–351.

Hogg, A. and D. Pritchard (2004). The effects of hydraulic resistance on dam-break and other shallow inertial flows. *J. Fluid Mech. 501*, 179–212.

Huang, X. and M. Garcìa (1998). A Herschel-Bulkley model for mud flow down a slope. *J. Fluid Mech. 374*, 305–333.

Iverson, R. and R. Denlinger (2001). Flow of variably fluidized granular masses across three-dimensional terrain. 1. Coulomb mixture theory. *J. Geophys. Res. 106*, 537–552.

McElwaine, J. (2005). Rotational flow in gravity current heads. *Philosophical Transactions of the Royal Society of London series A 363*, 1603–1623.

Parker, G., Y. Fukushima, and H. Pantin (1986). Self-accelerating turbidity currents. *J. Fluid Mech. 171*, 145–181.

Ritter, A. (1892). Die Fortpflanzung der Wasserwellen. *Zeit. Vereines Deutsch. Ing. 36*(33), 947–954.

Rottman, J. and J. Simpson (1983). Gravity currents produced by instantaneous releases of a heavy fluid in a rectangular channel. *J. Fluid Mech. 135*, 95–110.

Savage, S. and K. Hutter (1989). The motion of a finite mass of granular material down a rough incline. *J. Fluid Mech. 199*, 177–215.

Simpson, J. (1972). Effects of a lower boundary on the head of a gravity current. *J. Fluid Mech. 53*, 759–768.

Simpson, J. (1987). *Gravity Currents in the Environment and the Laboratory*. Chichester: Ellis Horwood Limited.

Stoker, J. (1957). *Water Waves*. New York: Interscience Publishers.

Whitham, G. (1954). The effects of hydraulic resistance in the dam-break problem. *Proc. Roy. Soc. London A 227*, 399–407.

Whitham, G. (1974). *Linear and Nonlinear Waves*. New York: John Wiley & Sons.